Friction **10**(12): 2000–2017 (2022)
https://doi.org/10.1007/s40544-021-0563-8
ISSN 2223-7690
CN 10-1237/TH
RESEARCH ARTICLE

Insight into macroscale superlubricity of polyol aqueous solution induced by protic ionic liquid

Zhiwen ZHENG[1,2], Xiaolong LIU[1], Hongxiang YU[1,2], Haijie CHEN[1,2], Dapeng FENG[1,*], Dan QIAO[1,*]

[1] *State Key Laboratory of Solid Lubrication, Lanzhou Institute of Chemical Physics, Chinese Academy of Sciences, Lanzhou 730000, China*

[2] *Center of Materials Science and Optoelectronics Engineering, University of Chinese Academy of Sciences, Beijing 100049, China*

Received: 18 August 2021 / Revised: 30 September 2021 / Accepted: 14 October 2021

Abstract: Currently, macroscale liquid superlubricity remains limited to low applied loads and typical ceramic friction pairs. In this study, a robust macroscale superlubricity with a coefficient of friction (COF) of approximately 0.006 is realized at the bearing steel interface induced by protic ionic liquids (ILs) in propylene glycol aqueous solution, and the lubrication system exhibits excellent anti-corrosion properties. Results show that superlubricity can be achieved by employing ILs with longer alkyl chains over a wide load (< 350 N) and speed (> 700 r/min) range. By systematically investigating factors affecting superlubricity, including the IL structure, ionization degree, test conditions, polyol, water-to-alcohol ratio, and lubrication state, the superlubricity mechanism is discussed. Notably, a thicker and denser stern layer can be formed using ILs with longer alkyl chains, which participates in the tribochemical reaction with the metal substrate to form a tribofilm during rubbing. The hydrogen bond network layer formed by the hydrogen ion and polycol aqueous solution can withstand high applied loads. Water can be used to reduce the shear stress of polyols, and enable superlubricity to be achieved under high-speed rotations. Moreover, an inevitable running-in period serves as a dispersing contact stress and dynamically forms a lubricating film, where the lubrication state locates mixed lubrication and then transforms into boundary lubrication as the roughness of the contact surface increases. This study is expected to significantly promote the development and application of superlubricity in the engineering field.

Keywords: macroscale superlubricity; ionic liquids (ILs); steel interface; corrosion; tribochemical reaction

1 Introduction

The macroscale friction and wear of machine devices with moving components, such as bearings or gears, remain challenging to the scientific and industrial communities because severe friction and wear issues contribute to more than 33% of energy consumption and 60% of machine breakdown worldwide [1]. Therefore, significant innovative efforts have been expended to reduce friction and wear, e.g., by applying lubricants, employing coating technology, and developing self-lubricating alloy materials [2–4]. In particular, superlubricity, which is considered the most promising strategy to minimize or eliminate frictional energy losses and wear-related material damage [5], has garnered significant immense attention since it was first proposed by Shinjo and Hirano in the 1990s [6]. Superlubricity is primarily considered to be a lubrication state with a coefficient of friction (COF) of less than 0.01 between two relatively sliding surfaces [7, 8]. Currently, superlubricity can be obtained at the non-liquid sliding interface with weak interfacial interactions using homogeneous graphite/graphite, graphene/graphene, MoS_2/MoS_2 and heterogeneous gold/graphite, graphite/hexagonal boron nitride, graphite/MoS_2 [9–11], etc., as well as carbon-based

* Corresponding authors: Dapeng FENG, E-mail: dpfeng@licp.cas.cn; Dan QIAO, E-mail: ddqiao@licp.cas.cn

film surfaces, such as amorphous carbon (a-C:H), diamond-like carbon, and tetrahedral amorphous carbon (ta-C) under specific structures and conditions [12–15]. Furthermore, superlubricity is primarily achieved between sliding interfaces with liquid as a medium, such as water, glycerin, polymer brush, ionic liquid, polyalphaolefin oil, biological liquid, and polyhydric alcohol solution with acids or two-dimensional (2D) additives [16–20].

Compared with solid superlubricity, which is achieved under harsh conditions such as unique surface textures, complex structure superlubricity, vacuum or specific atmospheric environments, limited atomically smooth films, and perfectly crystalline materials [21, 22], liquid superlubricity can be efficiently realized under normal operating conditions using suitable lubricants [23]. As such, liquid superlubricity offers more practical engineering application potential. In recent years, significant developments in liquid superlubricity have been achieved, particularly in water-based lubricant systems, owing to its appropriate viscosity–pressure coefficient [24]. Therefore, a series of water-based superlubricity systems have been investigated, including polyol aqueous solutions with acids, alkali metal ions, ionic liquids (ILs), and 2D materials, and the lubrication mechanism was revealed [25–29]. Currently, the mechanism of aqueous lubrication is primarily ascribed to 1) the hydration effect, which results in the low shear strength of the lubricant; 2) the adsorbed boundary layer established at the interface; 3) the hydrodynamic effect; 4) the tribochemical reaction between the substrate and lubricant; and 5) the running-in process for decreasing the contact pressure [30]. The achievement of superlubricity under boundary, mixed, and elastohydrodynamic lubrication has been reported [26, 31]. However, these liquid superlubricity systems offer limited achievements at low applied loads and low speeds as well as when ceramic friction pairs and ball-on-disc or pin-on-disc tribometers are used [32–34]. Considering the application of liquid superlubricity in most industrialized domains, the limitations associated with the applied load must be enhanced, friction pairs must be extended to bearing steel under ball-on-ball contact, and the corrosion resistance of water-based lubricants must be improved [35].

ILs, as room-temperature molten salts comprising cations and anions, possess multiple unique physical and chemical properties, such as nonflammability, super low volatility, wide electrochemical window, and high chemical and thermal stability, causing them to be used widely in the friction field [36]. The merits of ILs as lubricants or lubricant additives are primarily attributed to strong surface adsorption due to inherent polarity ions, tribochemical reactions involving active elements for forming a tribofilm, a strong lubricating film that resists loads, and excellent corrosion resistance [37, 38]. In particular, protic ILs can not only provide hydrogen ions to supply hydrated ions required for liquid superlubricity but also offer other advantages as a lubricant [39–41]. Combined with the intrinsic mechanism of liquid superlubricity, protic ILs have become one of the best candidates in superlubricity fields. Therefore, to overcome the current limitations of low loads and the use of friction pairs only to achieve superlubricity, in this study, protic ILs were employed as additives in a polyol aqueous solution. Excellent macroscale liquid superlubricity was realized for the first time under a high applied load (300 N, corresponding initial contact pressure of 2.1 GPa) for the ball-on-ball contact of bearing steel interfaces. This superlubricity state can be extended to a wide range of loads, speeds, and polyols, and can provide excellent corrosion resistance for water-based lubricating systems. By systematically investigating the factors that affect superlubricity behavior, involving hydration, adsorption, tribochemical reaction, running-in period, and changes in the lubricating state, the mechanism of macroscale liquid superlubricity was successfully revealed. Hence, the application and recognition of superlubricity between steel interfaces under high load and speed conditions can be expanded significantly.

2 Experimental

2.1 Materials

N,N-dimethylbutylamine, N,N-dimethyloctylamine, N,N-dimethyldodecylamine, and N,N-dimethylhexadecylamine (purity, 98%) were purchased from Shanghai Macklin Biochemical Co., Ltd., China. Bibutyl

phosphate (purity, 98%) was supplied by Sa En Chemical Technology Shanghai Co., Ltd., China. All polyols were obtained from Tianjin Ke Miou Chemical Reagent Co., Ltd., China. The other chemical reagents were of analytical grade and were used without further purification. Deionized water was prepared by the Lanzhou Institute of Chemical Physics, Chinese Academy of Sciences, China.

2.2 Preparation of protic ILs

As shown in Fig. 1, four protic ILs with different alkyl chains were synthesized via a proton transfer reaction between phosphate and alkanolamines. Briefly, equimolar dibutyl phosphate and different alkanolamines (DMA*n*, *n* = 4, 8, 12, 16) were added to a round-bottom flask containing 30 mL acetonitrile, purified three times with nitrogen, and heated in an oil bath at 65 °C for 12 h. Subsequently, the solvents were removed via distillation under reduced pressure, and then washed several times with anhydrous ether to obtain a light yellow oily liquid, which were marked as PDMA4, PDMA8, PDMA12, and PDMA16, respectively. The structure data of ILs are presented in Section 1 in the Electronic Supplementary Material (ESM).

2.3 Preparation of lubricant samples

Water-based lubricant samples were prepared by mixing 50 wt% 1,3-propanediol (PG) and 50 wt% deionized water (denoted as PG_{aq}). The prepared ILs were used as additives in PG_{aq} with mass ratios of 1%, 2%, 3%, 4%, and 5%, separately, and are denoted as IL-PG_{aq}. To investigate the effect of alcohol on the superlubricity system, several different monohydric or polyhydric alcohols, including isopropanol (IPA), ethylene glycol (EG), 1,2-propylene glycol (1,2-PG), 1,4-butylene glycol (BDO), glycerol (GI), and polyethylene glycol 200 (PEG200), were used as alcohols to investigate the lubrication performance of water-based lubricants with the addition of 4 wt% PDMA16, which are marked as IPA_{aq}, EG_{aq}, 1,2-PG_{aq}, BDO_{aq}, GI_{aq}, and $PEG200_{aq}$, respectively. Optical photographs captured during the preparation of the lubricant samples are shown in Fig. S1 in the ESM. After the IL was added, it was completely dissolved in a polyol aqueous solution. Subsequently, the sample bottle was shaken, and bubbles were generated owing to the surface activity of the protic ILs. Subsequently, ultrasonic treatment was performed for 2 min to remove bubbles from the liquid. A uniform and transparent lubricant sample was obtained. After storing for 5 d, the sample remained intact owing to the good miscibility of water, polyols, and the prepared ILs.

2.4 Friction and wear test

Friction experiments were conducted on a four-ball tribometer (MS-10 A, Lanzhou Huahui Instrument Technology Co., Ltd., China; accuracy of sensor, 10 mN; Fig. S2 in the ESM) to assess the lubrication performance of the samples. The test conditions were as follows: a rotary speed of 1,200 r/min (0.461 m/s, Table S1 in the ESM), and a constant load of 300 N (corresponding Hertz contact stress of 2.1 GPa) applied for 30 min under steel-to-steel contact (GCr 15, ϕ = 12.7 mm). In addition, variable speeds ranging from 700 to 1,700 r/min and variable loads ranging from 150 to 350 N were tested. Table S1 in the ESM lists the initial contact stress and sliding linear velocity corresponding to different loads and rotary speeds. All tests were performed at 25±3 °C and 30%–45% relative humidity, as well as being repeated three times to ensure reliability and precision.

2.5 Characterizations

The structures of the ILs were determined using the nuclear magnetic resonance (NMR; Bruker Avance III 400 MHz spectrometer, Switzerland) and the high resolution mass spectrometrer (HRMS; Bruker micrOTOF Q II, Switzerland). The density and kinematic

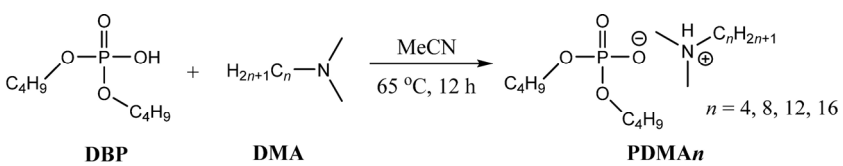

Fig. 1 Synthesis path of protic ILs.

viscosity of the lubricant samples at 25 °C were measured using a kinematic viscometer (SYP1003-III, Shanghai Instrument Group Co., Ltd., China). The electrochemical performance of the lubrication samples was tested using a three-electrode electrochemical workstation (PGSTAT 30, Metrohm, Sweden) on a Q235 steel surface with an exposed area of 1 cm^2. A QCM-D system equipped with four chambers was applied to probe IL additive adsorption at 25 °C via flow injection through separate Teflon tubes (inner diameter = 0.75 mm) to supply an aqueous solution with 2 wt% ILs using a peristaltic pump at a flow rate of 100 μL/s (QCM-D, Biolin Scientific, Sweden). Gold-coated quartz crystal sensors (QSX-301, Q-sense AB, Biolin Scientific, Sweden) were used. The wettability of the samples on a GCr15 steel surface was measured by depositing 5 μL of liquid on the surface using a DSA100 contact angle meter (KRUSS, Germany) at 25 °C. In addition, the morphologies of the worn surfaces were analyzed using the scanning electron microscope (SEM; JSM-5600LV, JEOL, Japan) and a three-dimensional (3D) profiler (MicroXAM-800, KLA-Tencor, USA). The chemical compositions of the worn surfaces were analyzed via the X-ray photoelectron spectrometer (XPS; ULVAC-PHI5000 Versaprobe III, Ulvac-Phi, Japan) and the time-of-flight secondary mass spectrometrer (TOF-SIMS; PHI nanoTOF II Time-of-Flight SIMS, Ulvac-Phi, Japan).

3 Results and discussion

3.1 Characterization of samples

Table 1 shows the density (ρ), kinematic viscosity (v), viscosity (η), and contact angle (CA) of PG_{aq} and PG_{aq} with 4 wt% of the four different ILs. The results show that after adding ILs to PG_{aq}, the change in density is slight when compared with the density of basic PG_{aq}. However, as the cationic alkyl chain lengthened, the viscosity of the lubricant samples increased gradually, whereas the contact angle decreased gradually. This can be attributed to the hydration ionization of protic ILs in the water–polyol solution arising from the interaction of hydrogen bonds. Furthermore, ILs with longer alkyl chains were more easily adsorbed on the steel surface, resulting in a better wettability of 4 wt% PDMA16-PG_{aq} on the steel surface. The viscosity and wettability of the steel surface of the lubricant samples may significantly affect the superlubricity.

Table 1 Density (ρ), kinematic viscosity (v), viscosity (η), and contact angle (CA) on GCr 15 steel surface of PG_{aq} and 4 wt% four ILs in PG_{aq} at 25 °C.

Item	PG_{aq}	4 wt% PDMA4	4 wt% PDMA8	4 wt% PDMA12	4 wt% PDMA16
ρ (g/mL)	1.035	1.038	1.034	1.033	1.029
V (mm^2/s)	3.07	3.69	3.79	3.92	4.57
η (mPa·s)	3.18	3.83	3.92	4.05	4.70
CA (°)	53.2	44.3	42.0	32.7	29.3

3.2 Friction test

Figure 2 shows the evolution of the COF curves with time, steady-state COF, and final contact pressure (FCP) lubricated by PG_{aq}, water with 4 wt% PDMA16, PG with 4 wt% PDMA16, and PG_{aq} with 4 wt% PDMA16. Corresponding photographs of wear scars, wear scar diameter (WSD), and 2D contours are shown in Figs. 2(c)–2(f). The steady-state COF was the average COF in which the running-in period of approximately 600 s was removed, and the FCP can be calculated by assigning the final WSD with Eq. (S1) in the ESM. The temperature of the oil box after the friction test is shown in Fig. S3 in the ESM. For the basic PG_{aq}, the average COF was approximately 0.32, and the friction curve exhibited significant oscillations (Fig. 2(a)). The high COF was due to the inferior lubrication of simple PG_{aq}, which hindered the formation of a good boundary lubricating film under a high load. However, the COF fluctuated significantly because water vapor was formed owing to the significant amount of heat released during the friction process. It was confirmed that the temperature outside the oil box reached 46.4 °C after the friction test, whereas the temperature of the oil box was higher, thereby causing a significant amount of PG_{aq} to evaporate. Optical photographs of the wear scars (Fig. 2(c)) show that the WSD was 0.868 mm and many deep scratches measuring approximately 6 μm formed on the wear surface (Fig. 2(g)). The FCP reached approximately 209 MPa (Fig. 2(b)).

When 4 wt% PDMA16 with long alkyl chains was added to water and PG, the average COFs were approximately 0.075, and the temperature of the oil

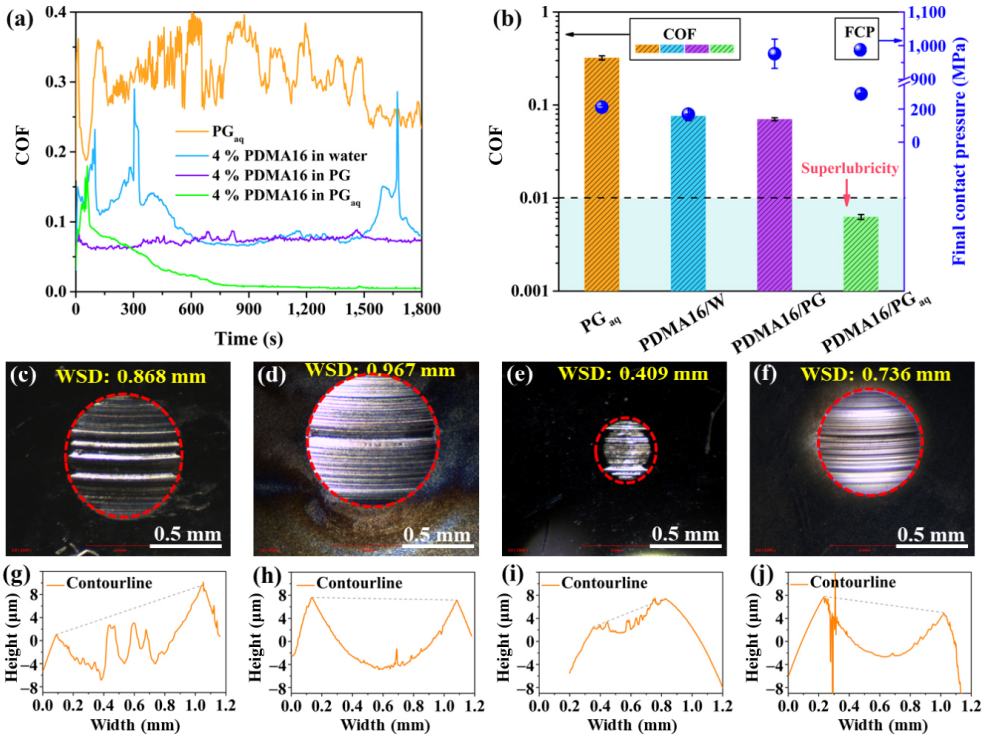

Fig. 2 (a) Evolution of COF curves with time and (b) average steady-state COF and final contact pressure (FCP) lubricated by PG_{aq}, 4 wt% PDMA16 in water, 4 wt% PDMA16 in PG, and 4 wt% PDMA16 in PG_{aq} under conditions of 300 N and 1,200 r/min within 1,800 s. (c–f) Corresponding photographs and WSDs of wear scars. (g–j) Corresponding 2D contour lines.

box did not increase after the test. However, the COF curve of PG was smoother than that of water, and the COF fluctuates significantly at the beginning and the end stages. In addition, water indicated the largest WSD of 0.967 mm, and its FCP was 165 MPa. Meanwhile, PG indicated the smallest WSD (0.409 mm), which results in a maximum FCP of 977 MPa. The irregular wear surface exhibited deep and wide furrows (Fig. 2(i)). Interestingly, when 4 wt% PDMA16 was added to PG_{aq}, the COF first increased significantly to 0.18 within approximately 60 s, and then quickly decreased to approximately 0.03 at 450 s. Next, the COF decreased gradually and finally entered a superlubricity state (COF < 0.01) at approximately 750 s. Subsequently, the COF fluctuated slightly between 0.003 and 0.007 until the end of the test. The average steady-state COF was approximately 0.006. The round wear scar indicated that the WSD was 0.736 mm and the FCP reachd 292 MPa. The wear surface was smooth, with only some shallow furrows (Fig. 2(j)). Hence, a robust macroscale superlubricity was achieved by adding 4 wt% PDMA16 to PG_{aq}.

To obtain further insight into the effects of the alkyl chain length and concentration of ILs on the lubricating performance, four ILs with different alkyl chain lengths were tested as additives in PG_{aq}, and their lubrication performances were evaluated under conditions of 300 N and 1,200 r/min, as shown in Fig. S4 in the ESM. Figure 3(a) shows the average COF and FCP of PG_{aq} with different additives. When PDMA4 and PDMA8 with shorter alkyl chains were used, the average COFs decreased to 0.014 and 0.027, respectively. Their WSDs were approximately 0.800 mm, which implies that the FCP was maintained at approximately 220 MPa. When PDMA12 and PDMA16 with longer alkyl chain were used, their COFs decreased to 0.01 and 0.006, respectively, indicating that macroscale superlubricity was achieved. Furthermore, the concentrations of ILs contributes significantly to the realization of superlubricity, as shown in Fig. 3(b). When a small amount of additives was used, such as 1 or 2 wt%, superlubricity was not attained despite the significant decrease in the COFs to 0.04 and 0.015. However, when the concentration of IL exceeded 3 wt%, superlubricity was achieved, with the COF ranging from 0.006 to 0.007. This may be because a certain

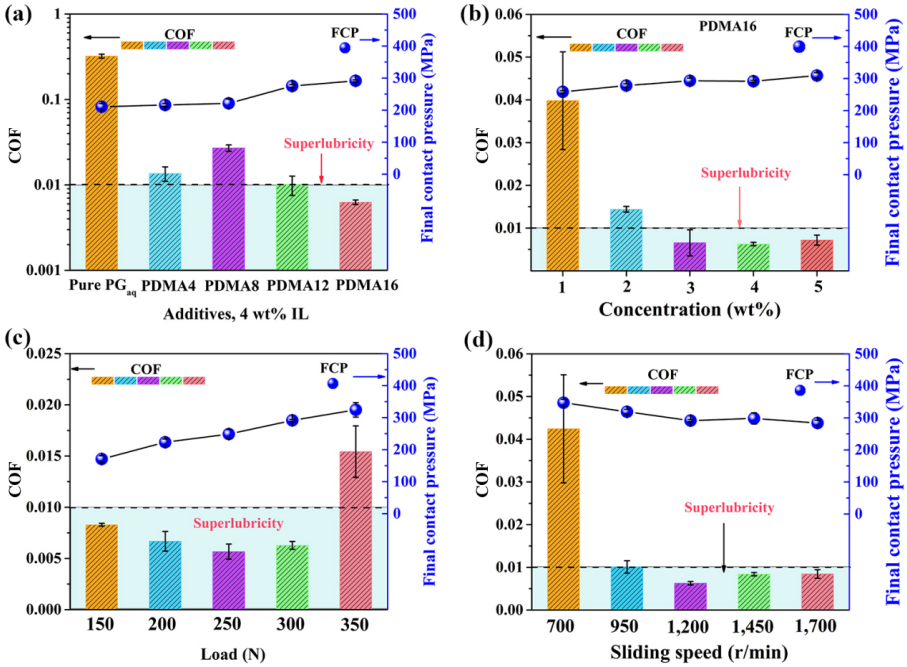

Fig. 3 Average steady-state COF and FCP of EG_{aq} (a) with different ILs with 4 wt% additive; (b) at various concentrations ranging from 1 to 5 wt% PDMA16 under 300 N and 1,200 r/min; (c) at various loads ranging from 150 to 350 N with 4 wt% PDMA16 at 1,200 r/min; (d) at various sliding speeds ranging from 700 to 1,700 r/min with 4 wt% PDMA16 and 300 N within 1,800 s.

amount of hydrogen ions was required to realize superlubricity [26, 29]. Therefore, macroscale superlubricity can be achieved using long alkyl chain ILs (> 12) at higher concentrations (> 2 wt%).

Figures 3(c) and 3(d) show the results from experiments involving various loads and variable sliding speeds for 4 wt% PDMA16 to provide a better understanding of the application range of the superlubricity system. When the loads were less than 350 N, superlubricity was achieved with the COFs between 0.006 and 0.008. For the higher load of 350 N, the COF increased to 0.015, indicating that increasing the load was not conducive to the achievement of superlubricity. Corresponding photographs and WSDs are shown in Fig. S5(a) in the ESM. The wear surface was bright and smooth, indicating that the water-based lubrication system barely corroded the steel interfaces, which may be attributed to the adsorption of the IL on the metal surface to prevent water corrosion. When the sliding speed was extremely low, e.g., 700 r/min, the COF was 0.042. When the sliding speeds increasd to 950–1,700 r/min, the superlubricity state was achieved again in the COF range between 0.01 and 0.006; this may be because the shear layer of lubricating film had to maintain a certain speed. Hence, it can be concluded that superlubricity can be achieved in a wide load (< 350 N) and sliding speed (> 700 r/min) range.

3.3 Characterization of wear scars

To determine how different ILs affected superlubricity, the morphologies of the worn regions lubricated by various concentrations of PDMA4 (non-superlubricity) were observed after performing a tribotest using a 3D profiler (Fig. 4). Therefore, the chemical composition of the wear scar based on 4 wt% PDMA4 was analyzed using XPS. When a lower concentration of PDMA4 was added into PG_{aq}, i.e., 1 and 2 wt%, the wear surface showed severe scratches and the WSDs reached 1.02 and 1.06 mm, respectively. As the concentration of the IL increased to 3 and 4 wt%, the worn surface became smoother, and the WSDs decreased to 0.85 and 0.80 mm, respectively; this may be caused by the formation of a denser IL adsorption film to prevent the direct contact of metal [42]. Furthermore, Fig. S6 shows XPS spectra of C 1s, N 1s, O 1s, P 2p, and Fe 2p detected from fresh steel ball surface before frictional tests. When IL was used as an additive, results from XPS analysis show that the peaks in the C 1s deconvolution spectrum were at 284.6, 285.4, 285.6, and 288.6 eV, which were attributed to adsorbed

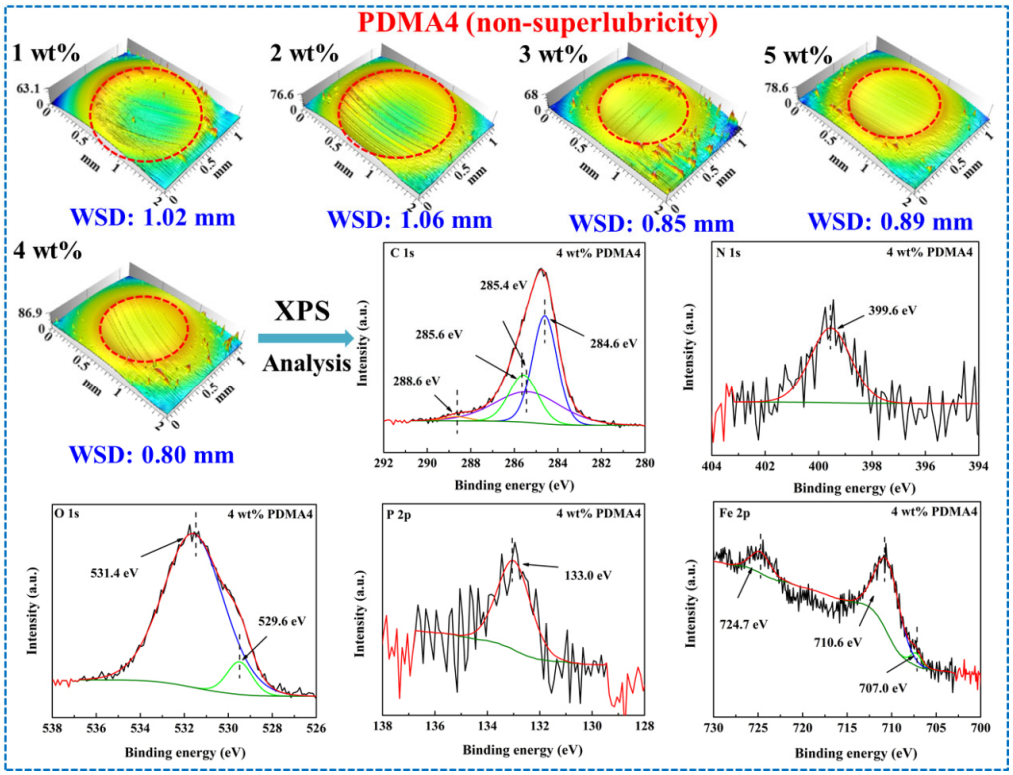

Fig. 4 3D micrographs of worn tracks lubricated by the blend with PDMA4 as additive in PG_{aq} under conditions of 300 N and 1,200 r/min within 1,800 s. XPS spectra of N 1s, O 1s, P 2p, and Fe 2p from wear scars lubricated by PG_{aq} with 4 wt% PDMA4.

carbon, C–C, C–O, and C=O bonds, respectively [43]. The N 1s peak at 399.6 eV was assigned to N–C bonds, including CN and CNO functional groups. Other peaks of O 1s at 531.4 and 529.6 eV can be attributed to iron oxide, carbon oxide, or phosphorus oxide. The single P 2p peak that appeared at 133 eV can be attributed to phosphates PO_4^{3-}, PO_2^-, or H_2PO^-. The Fe 2p peaks at 707.0, 710.6, and 724.7 eV were attributed to Fe(OH)O and iron oxides, including Fe_2O_3, Fe_3O_4, and FeO [44]. The results show that the IL can participate in the tribochemical reaction of the contact surface to form a tribofilm.

Compared with the short-chain PDMA4, when the long-chain PDMA16 was used, the 3D micrographs of worn tracks (Fig. 5) indicated that even at low concentrations, the wear scars presented shallower and narrower grooves, which may be because the IL with a long alkyl chain was able to form a thicker adsorption film. Therefore, even at low concentrations, it can effectively avoid direct contact between friction pairs [42]. In addition, when the addition amount of PDMA16 was 1–5 wt%, the WSDs were similar, which indicates that the realization of superlubricity not only depended on the adsorption of ILs on the metal surface but also on the degree of hydration ionization of the PG aqueous solution [29]. Similarly, the chemical composition of the wear surface lubricated by PG_{aq} with 4 wt% PDMA16 was analyzed using XPS (Fig. 5). Compared with PDMA4, a new peak was detected at 283.2 eV in the C 1s spectrum, which was attributed to the C–N bond of carbonitride [38]. For the N 1s spectrum, another peak at 397.7 eV was observed, which can be assigned to N–O. This can be further confirmed by the O 1s peak at 532.3 eV assigned to nitrogen oxides. Hence, the results indicate that a thicker and denser adsorption layer can be formed using ILs with longer alkyl chains on the surface of the metal substrate. The adsorption layer can not only avoid the direct contact of the friction pair but also cause a tribochemical reaction at a more vigorous level to form a smooth tribofilm.

A TOF-SIMS test was performed to investigate the tribofilm on the worn surface. Figure 6 shows that the TOF-SIMS mass spectra of cations and anions derive from the tribofilm with 4 wt% PDMA4 (non-superlubricity) and 4 wt% PDMA16 (superlubricity),

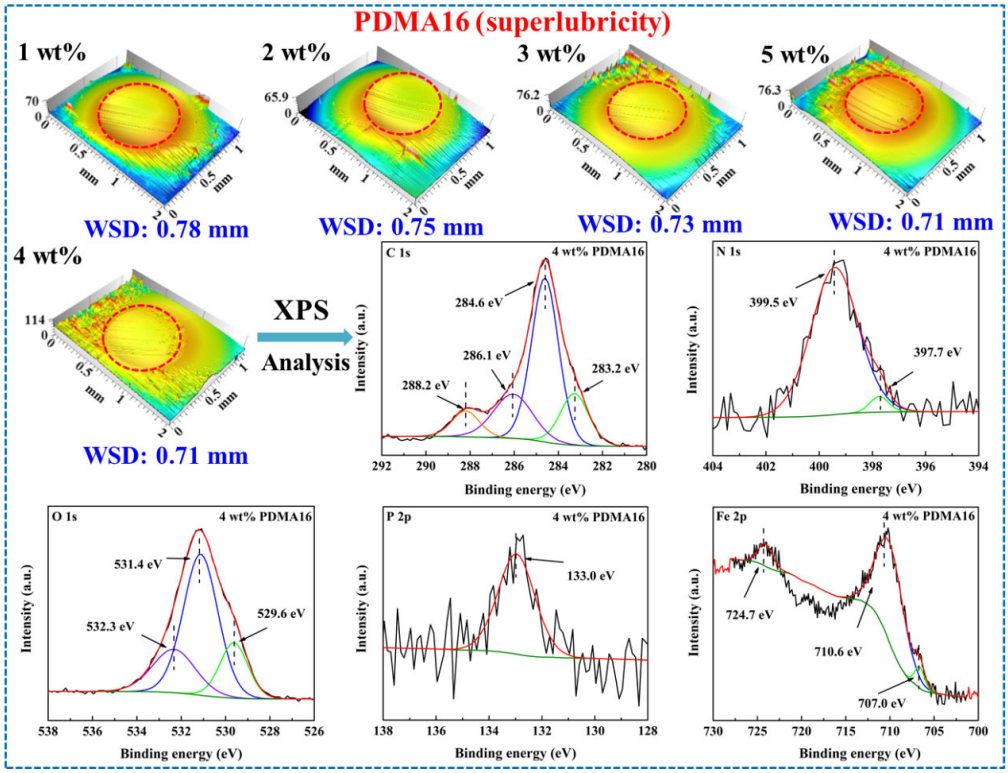

Fig. 5 3D micrographs of worn tracks using different concentrations of PDMA16 under conditions of 300 N and 1,200 r/min within 1,800 s. XPS spectra of N 1s, O 1s, P 2p, and Fe 2p from wear scars lubricated by PG_{aq} with 4 wt% PDMA16.

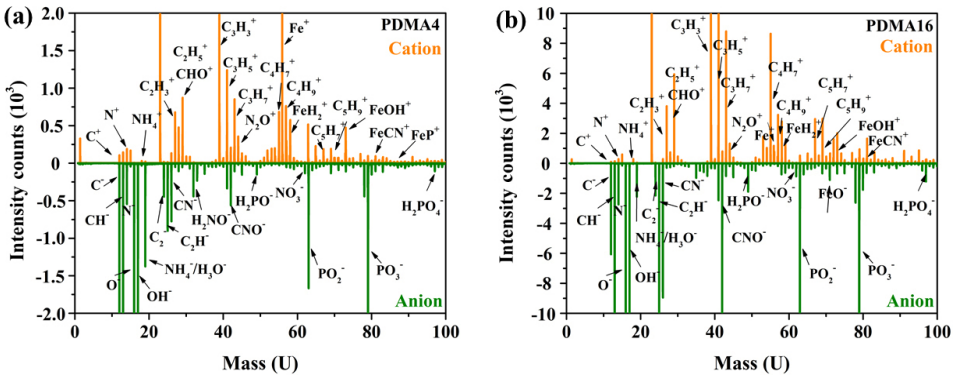

Fig. 6 TOF-SIMS mass spectra of cations and anions derived from tribofilm on steel worn surface lubricated by PG_{aq} with 4 wt% (a) PDMA4 and (b) PDMA16.

separately. The corresponding 2D TOF-SIMS images and fragment ion intensities are shown in Fig. S7 in the ESM and Fig. 7, respectively. In the mass spectra, different mass-charge ratios imply different ion fragments. Similar ion fragments were detected on the two worn surfaces with different ILs. For the cation spectra, a significant number of hydrocarbon ionic fragments ($C_xH_y^+$) arising from IL additives were identified, indicating that the long alkyl chain of the cation can be decomposed into shorter fragments during rubbing, which confirmed the occurrence of tribochemical reactions. In addition, ionic fragments with *m*/*z* 14 assigned as N^+, *m*/*z* 18 attributed to NH_4^+, and *m*/*z* 44 corresponding to N_2O^+ were identified, indicating that the tribofilm contains a significant amount of nitride.

For the anionic results of the two worn surfaces, similar characteristic peaks, including those representing nitrides, oxides, and phosphides, were identified, e.g., N^-, CN^-, CNO^-, NO^-, NO_3^-, O^-, OH^-, CH^-, H_2PO^-,

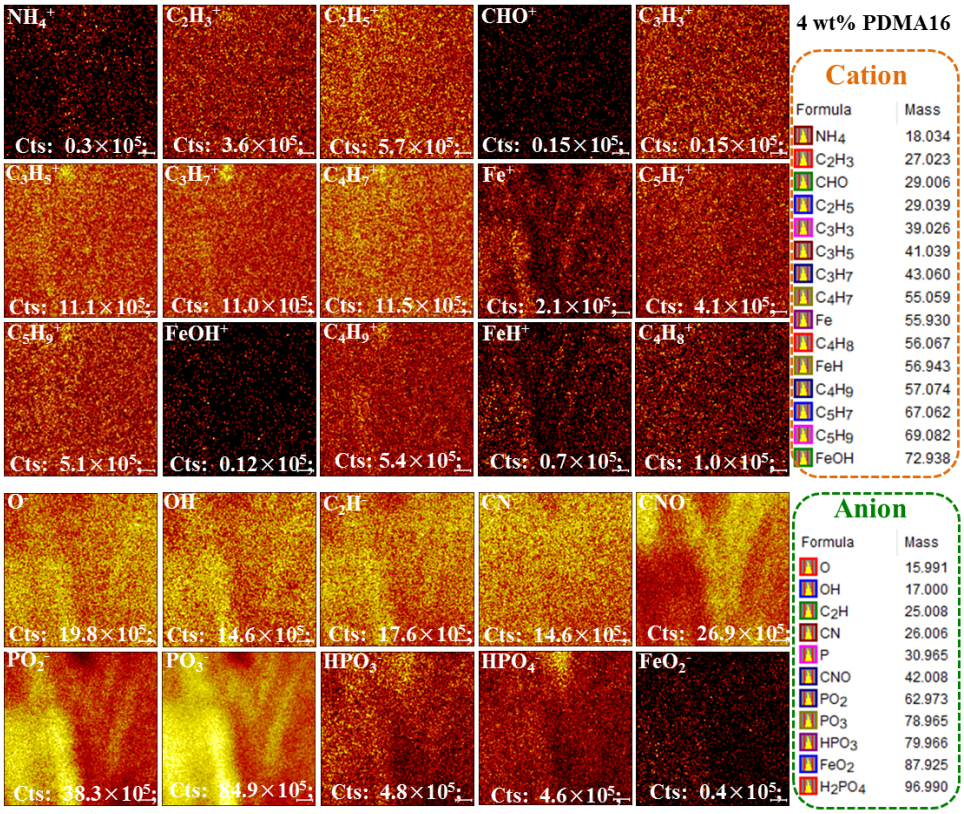

Fig. 7 2D TOF-SIMS images and fragment ion intensities of cations and anions derived from tribofilm on steel worn surface lubricated by PG_{aq} with 4 wt% PDMA16.

PO_2^-, PO_3^-, and $H_2PO_4^-$. Combined with the typical ion fragments of Fe (Fe^+, FeH_2^+, $FeOH^+$, $FeCN^+$, and FeO^-), it is discovered that a tribochemical reaction occurred between the ILs and the steel substrate. Consequently, a tribofilm composed of iron oxides, phosphate ferrites, and nitrogen ferrites was created, which prevented the further wear of the substrate. However, for ILs with different alkyl chain lengths, the degree of tribochemical reaction differed. This was manifested as a difference in the intensity of the fragmented ions, which can be visually reflected by the light level of 2D TOF-SIMS images. It was clear that the intensities of these characteristic fragmented ions ($C_xH_y^+$, C_2H^-, OH^-, CN^-, CHO^-, PO_2^-, PO_2^-, PO_2^-, and PO_2^-) derived from the tribofilm using PDMA16 were higher than those of PDMA4. Moreover, the intensity of Fe ions, such as Fe^+, $FeOH^+$, and FeH^+, was higher on the worn surface containing PDMA4, implying that more metal substrates were exposed after the non-superlubricity test. Hence, the XPS and TOF-SIMS results indicate that complex tribochemical reactions between the ILs and metal substrates occured during rubbing and yielded a tribofilm on the contact region. However, when ILs with longer alkyl chains were used, i.e., to achieve superlubricity, the degree of tribochemical reaction was higher, which might be associated with the thicker adsorption layer of long alkyl chains on the metal substrates [42, 45].

3.4 Characterization of surface adsorption

A quartz crystal microbalance (QCM) is an effective equipment for surface analysis that has been widely used to investigate the adsorption properties of organic molecules or ions on the surface of a substrate [46]. The operating principle of the QCM can be expressed by the Sauerbret equation (Eq. (1)) as Eq. (1):

$$\Delta f = \frac{2f_0^2}{A\sqrt{\rho\mu}}\Delta m \tag{1}$$

where the frequency change (Δf) is proportional to the adsorption quality (Δm), and $\frac{2f_0^2}{A\sqrt{\rho\mu}} = -0.28$ associated with the instrument. As presented in Fig. 8,

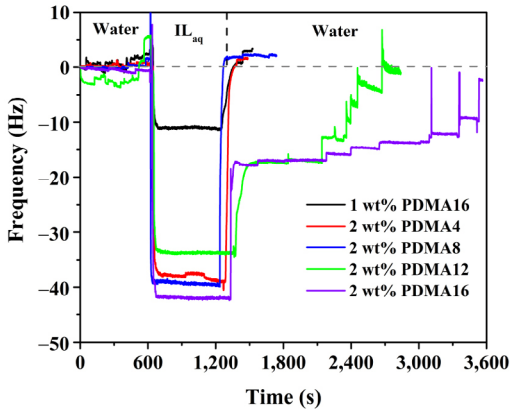

Fig. 8 Changes in frequency and corresponding dissipation of QCM gold chip for different ILs (using water as baseline).

when using 1 wt% PDMA16 in water, Δf was 11 Hz, and the frequency return to the baseline after pure water was used. By increasing the amount of IL additives to 2 wt% of PDMA4 and PDMA8 with shorter alkyl chains, the Δf value was approximately 38 Hz, and their frequencies returned promptly to the baseline, indicating the weak adsorption strength of ILs with shorter alkyl chains on the metal surface. For PDMA12 and PDMA16 with longer alkyl chains, the Δf values were 33 and 42 Hz, respectively. Interestingly, when solvent washing was performed, the frequency first returned to approximately 17 Hz. Subsequently, as the solvent continued to be washed, Δf decreased stepwise. When PDMA12 was used as an additive, Δf finally returned to the baseline at about 45 min; whereas when PDMA16 was used as an additive, Δf was going to the baseline at approximately 60 min. These results indicate that the adsorption strength of the ILs with low concentrations or short alkyl chains was low, which causes the adsorption layer to be easily destroyed and hindered the achievement of superlubricity. The ILs with long alkyl chains at high concentrations indicated a high adsorption strength on the metal surface. The adsorption layer was stable and not easily destroyed, which may have contributed to the achievement of superlubricity.

The electrochemical performance reflects not only the adsorption characteristics of the ILs on the metal surfaces but also the corrosion characteristics of the liquid lubricants, which are the most important performance indicator for water-based lubricants. As shown in Fig. 9, the polarization and impedance curves of the steel surfaces in different samples were tested. For basic PG$_{aq}$, the corrosion potential and corrosion current were −0.54 V and 6.95×10^{-3} A, respectively. After adding the ILs, the corrosion potential increased, whereas the corrosion current decreased, proving that the ILs can form an adsorption layer on the metal surface, thereby significantly improving the corrosion resistance of the water-based lubricants. However, as the alkyl chain length of the ILs increased, the corrosion potential increased gradually, indicating that the longer the alkyl chain rendered it easier for the ILs to obtain a stable and thick protective layer on the metal surface. The radius of curvature of the impedance curves can prove the corrosion resistance of the liquid. As shown in Fig. 9(b), the impedance radius of curvature of PG$_{aq}$ was the smallest. After adding the ILs, the radius of the impedance curvature increased with the alkyl chain length of the ILs. Similarly, the adsorption performance and anti-corrosion performance increased with the concentration of the ILs, as shown in Fig. S8 in the ESM. Therefore, the adsorption of ILs on the metal surface improved not only the lubricating performance but also the corrosion resistance.

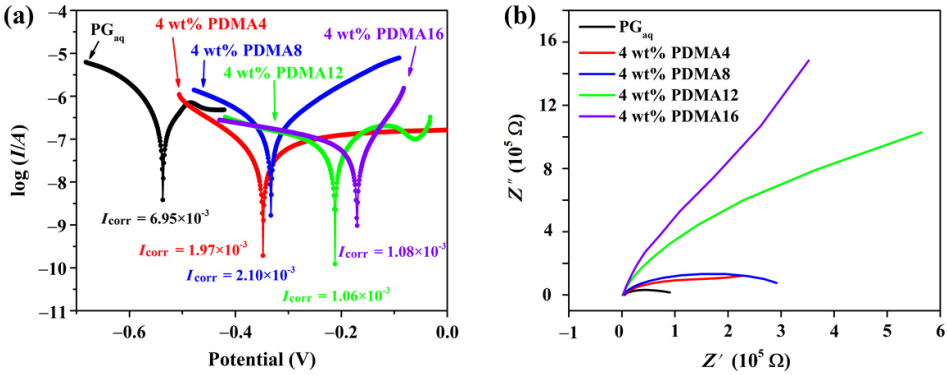

Fig. 9 (a) Polarization curves and (b) impedance curves of Q235 carbon steel in PG$_{aq}$ and in the blends with different additives in PG$_{aq}$.

3.5 Effects of liquid properties on superlubricity

To further investigate the effects of the CA and viscosity characteristics of the lubricants on superlubricity, lubricant samples with various mass ratios of water to PG using 4 wt% PDMA16 (W/PG) were tested. The details are listed in Table S3 in the ESM, and the results are presented in Fig. 10. The change trend of the CA was wavy with a water-to-alcohol ratio from 10:0 to 0:10. The viscosity first decreased, and then increased. For example, when W/PG was 10:0, CA decreased to 27°, whereas the viscosity was the highest at 135 mPa·s, which may be attributed to the hydration between the IL and water due to hydrogen bonding. When the W/PG was 7:3 and 2:8, the values of CA were 59° and 54°, respectively. Meanwhile, the viscosity decreased to 7 and 18 mPa·s, respectively, and the COFs were 0.022 and 0.015, respectively. When the W/PG were 5:5 and 4:6, the CA and viscosity were approximately 28° and 8 mPa·s, respectively, and the COFs were 0.006 and 0.002, respectively. It was observed that when the W/PG was extremely high or too low, superlubricity was unachievable.

Furthermore, an experiment involving various concentrations of ILs with a water/PG mass ratio of 1:1 was performed to compare the effects of IL concentration, and the results are shown in Table 2. As the concentration of IL increased from 1 to 5 wt%, despite the viscosity of the samples increasing to 6.12 mPa·s, it remained at a low level, which ensured that the sample has a lower stress under high-speed shear. The CA of the samples on the steel surface decreased, indicating that the increase in concentration might have enhanced the wettability of the sample on the steel surface. Furthermore, when the IL concentration was greater than or equal to 3 wt%, the viscosity and CA of the sample were in an appropriate range, which allowed superlubricity to be achieved (Fig. 3(b)). Hence, superlubricity can only be achieved under both the appropriate wetting and suitable viscosity. In addition, as the proportion of PG increased, the FCP increased gradually, indicating that alcohol can reduce wear, although an excessive amount of alcohol will destroy the superlubricity.

To investigate the effect of alcohol on superlubricity, several typical alcohols, including monoalcohols (IPA), diols (EG, 1,2-PG, BDO), triols (GI), and polyols (PEG200), were used instead of PG, as shown in Fig. 11 and Table S4 in the ESM. The results show that the structure of polyol is an important internal factor for achieving superlubricity; in fact, it may be associated with the network formed by directional intermolecular hydrogen bonds O–H···O and the hydrated molecular units formed between the polyol aqueous solution

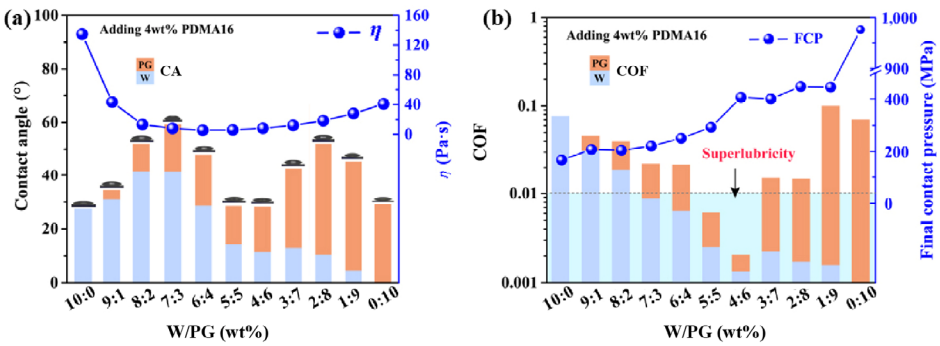

Fig. 10 Effects of lubricants with different mass ratios of water to PG with 4 wt% PDMA16 on superlubricity: (a) CA on surface of GCr15 steel and viscosity (η) at 25 ℃; (b) average COF and corresponding FCP under conditions of 300 N and 1,200 r/min within 1,800 s.

Table 2 Density (ρ), kinematic viscosity (ν), viscosity (η), and contact angle (CA) on GCr 15 steel surface of the blends with different concentrations of PDMA16 in PG_{aq} (1/1 wt%) at 25 ℃.

Item	1 wt%	2 wt%	3 wt%	4 wt%	5 wt%
ρ (g/mL)	1.034	1.031	1.029	1.029	1.026
ν (mm^2/s)	3.23	3.56	3.95	4.57	5.84
η (mPa·s)	3.34	3.67	4.06	5.90	6.12
CA (°)	55.2	48.7	33.4	29.3	22.4

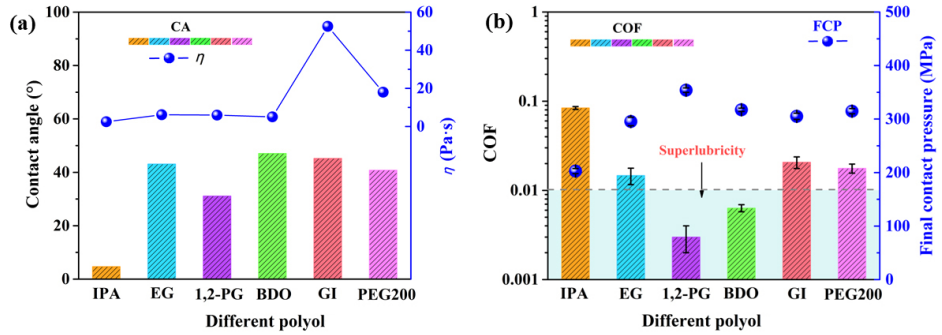

Fig. 11 Effects of different polyols on superlubricity for 4 wt% PDMA16: (a) CA of lubricants on surface of GCr15 steel and corresponding viscosity; (b) average COF and corresponding FCP under conditions of 300 N and 1,200 r/min.

and the ILs [47–49]. When only one hydroxyl group is presented, it is difficult to form a hydrogen-bond network and hydrated molecular units to resist high-speed-rotation friction pairs, e.g., IPA. When two hydroxyl groups are presented in the molecular structure, a hydrogen bond network can be formed easily among the hydroxyl groups [50, 51]. Moreover, the formed hydrated molecular unit exhibited the appropriate strength and shear in resisting the high-speed-rotation friction pair to achieve superlubricity, e.g., PG, 1,2-PG, and BDO. For the triols and polyols, GI_{aq} indicated the highest viscosity, which was attributed to its strong hydrogen bonding interactions. $PEG200_{aq}$ indicated a medium viscosity. Although its CA was in a decent range, superlubricity was not obtained. Therefore, if three or more hydroxyl groups are presented in the molecular structure, a strong hydrogen bond will result in a significant increase in viscosity, which is not conducive to the realization of superlubricity.

3.6 Evaluation of superlubricity

A segmented experiment was implemented to investigate the evolution of the superlubricity process more comprehensively. Based on the COF, five characteristic state points at 90, 310, 1,080, 1,800, and 3,600 s were selected (Fig. 12(a)). Subsequently, using

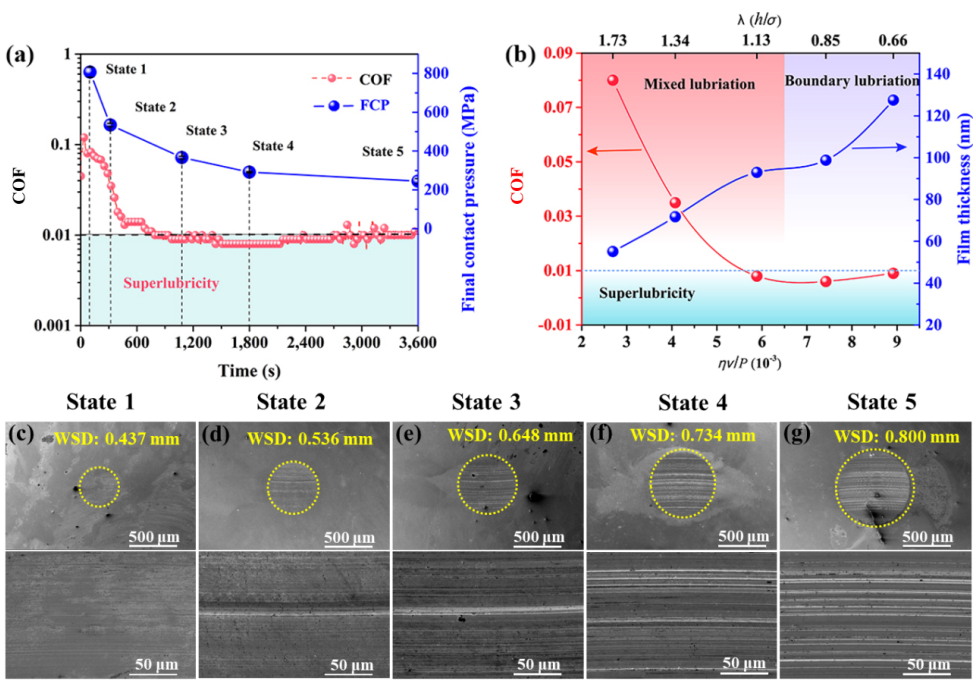

Fig. 12 (a) Evolution of COF and FCP with time. (b) Stribeck curve, lubrication film thickness, and λ as a function of Sommerfeld number ($\eta v/p$) at 90, 310, 1,080, 1,800, and 3,600 s, respectively. (c–g) Corresponding TEM images of worn tracks at different states, lubricated by 4 wt% PDMA16 under conditions of 300 N and 1,200 r/min.

the Stribeck theory and the minimum film thickness theory, the curve of the lubricating film thickness can be plotted, and the lubrication region at different states can be distinguished, as shown in Fig. 12(b), which provided a direct evidence of the superlubricity process.

The Stribeck curve depicts the changes in the COF based on the Sommerfeld number, which is defined as $\eta v/p$, where η, v, and p represent the viscosity, sliding velocity, and contact pressure, respectively [37]. The theoretical thickness (h_c) of the liquid lubricating film can be calculated using the Hamrock–Dowson theory of elastohydrodynamic lubrication of point contacts [52] as Eq. (2):

$$h_c = 2.69\frac{G^{0.53}U^{0.67}R}{W^{0.067}}(1-0.61e^{-0.73k}) \quad (2)$$

where $G=\alpha E$, $U=\eta v/ER$, and $W=F/ER^2$ are the dimensionless material elastic modulus, speed, and load, respectively. α is the pressure–viscosity coefficient of the lubricant; E is the effective elastic modulus of the friction pair; R is the effective radius of the ball; and F is the load. The lubrication regime can be determined using the ratio of the theoretical minimum film thickness (h_c) to the combined composite surface roughness (σ) as Eq. (3):

$$\lambda=\frac{h_c}{\sigma}=\frac{h_c}{\sqrt{\sigma_1^2+\sigma_2^2}} \quad (3)$$

where σ_1 and σ_2 are the roughness values of the contacting surfaces. The meanings and values of the variables in Eqs. (2) and (3) are provided in Section 5 in the ESM [53]. Table S5 in the ESM lists the theoretical thicknesses (h_c) of the liquid lubricating film, the roughnesses of the contacting surfaces (σ), and film thickness ratioes (λ) based on Eqs. (2) and (3).

It is discovered that in liquid superlubricity, a running-in period of approximately 450 s is inevitable. At state 1, the COF decreased to 0.08, and the contact stress was reduced from the initial 2.1 GPa to 806 MPa due to wear. Meanwhile, λ was 1.73, indicating that lubrication occured in the mixed lubrication area. At state 2, the COF decreased to 0.035. A few deep grooves appeared on the worn surface. After the running-in period, the COF decreased gradually to less than 0.01. In the initial stage of superlubricity, such as state 3, the COF decreased to 0.008, and a significant number of slight furrows appeared on the worn region. In the stable superlubricity phase (state 4), the COF was stable at approximately 0.007. The WSD increased to 0.734 mm, accompanied by more and deeper furrows in the wear area. Meanwhile, λ decreased to 0.85, indicating that the lubrication state was transformed into boundary lubrication. At state 5, more and deeper furrows evolved in the worn area, and the COF fluctuated at approximately 0.01. However, the WSD increased progressively to 0.8 mm within 1,800 s, indicating that only slight wear occurred during this period. Therefore, the evolution of superlubricity can be summarized as follows: 1) Severe wear in the initial stage resulted in a higher COF, and the contact stress decreased as the contact area increased. 2) Wear occured primarily during the running-in period and the initial stage of superlubricity, whereas the roughness of the worn surface increased gradually as the experiment progressed. 3) The lubrication state changed from mixed lubrication to boundary lubrication during a period of stable superlubricity.

As the lubrication system will cause greater damage to the equipment during the start–stop period, four start–stop tests were performed after a running-in period to investigate the friction state of this superlubricity system in the start–stop period, as shown in Fig. 13. It was observed that the COF fluctuated during the start–stop period, although it remained within the superlubricity level and stabilized quickly. This shows that the changes in the system state, such as

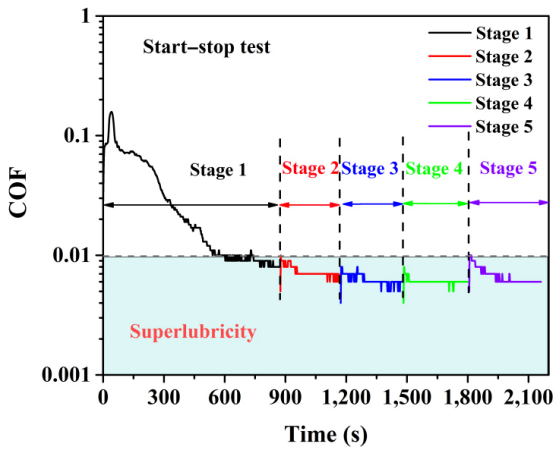

Fig. 13 Start–stop experiment after running-in period based on 4 wt% PDMA16 under conditions of 300 N and 1,200 r/min.

the speed of acceleration, the regeneration of the lubricating film, and the new contact pressure, do not significantly affect the superlubricity during the start–stop period.

3.7 Mechanism of superlubricity

Based on the aforementioned experimental results and discussion, a feasible superlubricity mechanism is foreseen for this superlubricity system, as depicted in Fig. 14. In the microscopic area between the contact interfaces (Fig. 14(c)), the overflow of free electrons on the metal surface caused the metal surface to be positively charged. Subsequently, the IL was adsorbed on the metal substrate through electrostatic interactions, and a Stern layer was generated [47–50]. This adsorption layer contained a liquid lubricating film, which guaranteed the corrosion resistance of the metal substrate. The ILs participated in the mechanical tribochemical reaction with the substrate to form a tribofilm. Furthermore, the combination of PG and protic ILs formed a hydrogen-bond network layer between PG and water on the Stern layer after the running-in process and served primarily as a bearing. Therefore, it can be deduced that some polyhydroxy alcohols, which can also form a similar hydrogen-bond network with water, can result in macroscale superlubricity when the appropriate protic ILs or hydrogen ions are used [48]. Currently, three types of diols have been validated in terms of their ability to achieve superlubricity; this ability may be attributed to the harmonious hydrogen bond network formed by the two hydroxyl groups and water molecules. In addition, the proportion of water and the concentration of hydrogen ions affect the viscosity of the mixture, which may reduce the shear strength of the shear layer during high-speed rotations. These comprehensive effects enable macroscale superlubricity to be achieved under a high applied load and high-speed rotations on a steel interface.

Figures 14(d)–14(f) show the evolution of the wear surfaces during rubbing. During the running-in period (states 1 and 2), the smoother wear surface caused lubrication to occur in the mixed lubrication area owing to significant flaking. Abrasion occurred primarily during this period, and resulted in a considerable decrease in the contact stress. In the early superlubricity, namely states 2 and 3, some furrows appeared on the wear surface, which caused the lubrication state to change from mixed lubrication to boundary lubrication, and the tribofilm was dynamically formed and consumed. Subsequently, friction entered the stable superlubricity stage (state 5), during which the lubrication was boundary lubrication.

4 Conclusions

In this study, the macroscale superlubricity of a steel interface under high applied loads and high-speed rotations was realized through the hydration ionization of protic ILs in polyol aqueous solution. By screening four ILs with different alkyl chain lengths, it is discovered that PDMA12 and PDMA16 with longer alkyl chains can achieve superlubricity when the addition amount exceeded 2 wt% in a diol aqueous

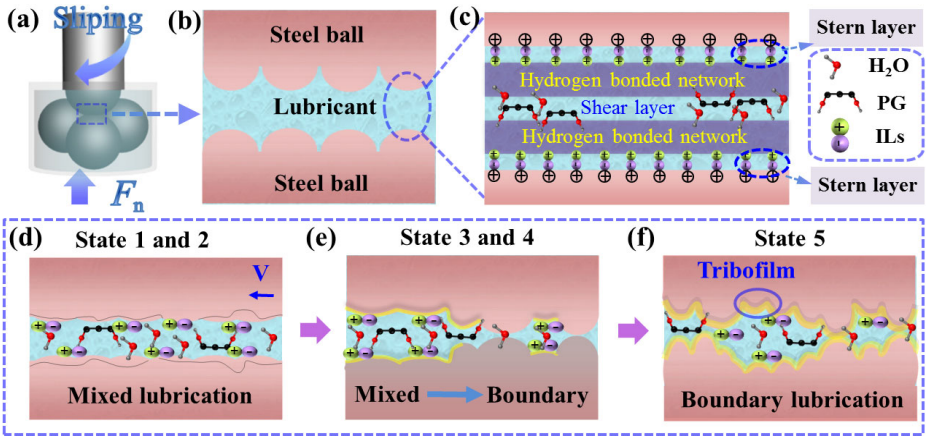

Fig. 14 (a) Schematic diagram of contact form for steel–steel contacts. (b, c) Schematic illustration of contact zones between steel–steel interfaces with lubrication of ILs in PG_{aq}. (d–f) Schematic illustration of evolution of wear surface at different stages.

solution. This superlubricity system can be applied to test conditions of less than 350 N and more than 700 r/min. In addition, some organic carbides, nitrides, phosphides, and iron oxides were identified on the wear surface, indicating that a complex tribochemical reaction occurred between the IL and the metal substrate, resulting in the formation of a tribofilm during the rubbing process. Adsorption experiments indicated that ILs with longer alkyl chains exhibited stronger adsorption, which resulted in the formation of thicker and denser Stern layers on the surface of steel. These adsorption layers not only intensified the tribochemical reaction but also assisted in the formation of a lubricating film to achieve superlubricity. In addition, the ratio of water to alcohol and the types of alcohol were crucial in achieving superlubricity. A segmented experiment showed that wear occurred primarily during the running-in period and the initial stage of superlubricity. The lubrication state transformed from mixed lubrication to boundary lubrication. Therefore, this study not only extended the macroscale superlubricity to high loads and high speeds but also analyzed the factors affecting liquid superlubricity systematically. Hence, insights into superlubricity under high loads and speeds were provided.

Acknowledgements

This work was supported by the Youth Innovation Promotion Association of Chinese Academy of Sciences (No. 2021422).

Electronic Supplementary Material Supplementary material is available in the online version of this article at https://doi.org/10.1007/s40544-021-0563-8.

References

[1] Holmberg K, Erdemir A. Influence of tribology on global energy consumption, costs and emissions. *Friction* **5**(3): 263–284 (2017)

[2] Cai M R, Yu Q L, Liu W M, Zhou F. Ionic liquid lubricants: When chemistry meets tribology. *Chem Soc Rev* **49**(21): 7753–7818 (2020)

[3] Zhang Z Y, Du Y F, Huang S L, Meng F N, Chen L L, Xie W X, Chang K K, Zhang C H, Lu Y, Lin C T, et al. Macroscale superlubricity enabled by graphene-coated surfaces. *Adv Sci* **7**(4): 1903239 (2020)

[4] Chen Z F, Yan H, Zhang P L, Yu Z S, Lu Q H, Guo J L. Microstructural evolution and wear behaviors of laser-clad Stellite 6/NbC/h-BN self-lubricating coatings. *Surf Coat Technol* **372**: 218–228 (2019)

[5] Luo J B, Zhou X. Superlubricitive engineering—Future industry nearly getting rid of wear and frictional energy consumption. *Friction* **8**(4): 643–665 (2020)

[6] Hirano M, Shinjo K. Atomistic locking and friction. *Phys Rev B Condens Matter* **41**(17): 11837–11851 (1990)

[7] Werne J, DeLuca E E, Rosner R, Cattaneo F. Development of hard-turbulent convection in two dimensions: Numerical evidence. *Phys Rev Lett* **67**(25): 3519–3522 (1991)

[8] Martin J M, Erdemir A. Superlubricity: Friction's vanishing act. *Phys Today* **71**(4): 40–46 (2018)

[9] Deng H, Ma M, Song Y M, He Q C, Zheng Q S. Structural superlubricity in graphite flakes assembled under ambient conditions. *Nanoscale* **10**(29): 14314–14320 (2018)

[10] Li H, Wang J H, Gao S, Chen Q, Peng L M, Liu K H, Wei X L. Superlubricity between MoS_2 monolayers. *Adv Mater* **29**(27): 1701474 (2017)

[11] Yaniv R, Koren E. Robust superlubricity of gold–graphite heterointerfaces. *Adv Funct Mater* **30**(18): 1901138 (2019)

[12] Ru G L, Qi W H, Tang K W, Wei Y R, Xue T W. Interlayer friction and superlubricity in bilayer graphene and MoS_2/$MoSe_2$ van der Waals heterostructures. *Tribol Int* **151**: 106483 (2020)

[13] Shi J, Xia T D, Wang C B, Yuan K, Zhang J Y. Ultra-low friction mechanism of highly sp^3-hybridized amorphous carbon controlled by interfacial molecule adsorption. *Phys Chem Chem Phys* **20**(35): 22445–22454 (2018)

[14] Yin X, Zhang J, Luo T, Cao B Q, Xu J X, Chen X, Luo J B. Tribochemical mechanism of superlubricity in graphene quantum dots modified DLC films under high contact pressure. *Carbon* **173**: 329–338 (2021)

[15] Berman D, Erdemir A, Sumant A V. Approaches for achieving superlubricity in two-dimensional materials. *ACS Nano* **12**(3): 2122–2137 (2018)

[16] Li J J, Cao W, Li J F, Ma M, Luo J B. Molecular origin of superlubricity between graphene and a highly hydrophobic surface in water. *J Phys Chem Lett* **10**(11): 2978–2984 (2019)

[17] Long Y, Kuwahara T, de Barros Bouchet M I, Ristić A, Dörr N, Lubrecht T, Dupuy L, Moras G, Martin J M, Moseler M. *In situ* synthesis of graphene nitride nanolayers on glycerol-lubricated Si_3N_4 for superlubricity applications. *ACS Appl Nano Mater* **4**(3): 2721–2732 (2021)

[18] Zhang Y X, Rutland M W, Luo J S, Atkin R, Li H. Potential-dependent superlubricity of ionic liquids on a graphite surface. *J Phys Chem C* **125**(7): 3940–3947 (2021)

[19] Zeng Q F, Yu F, Dong G N. Superlubricity behaviors of Si_3N_4/DLC films under PAO oil with nano boron nitride additive lubrication. *Surf Interface Anal* **45**(8): 1283–1290 (2013)

[20] Reddyhoff T, Ewen J P, Deshpande P, Frogley M D, Welch M D, Montgomery W. Macroscale superlubricity and polymorphism of long-chain *n*-alcohols. *ACS Appl Mater Interfaces* **13**(7): 9239–9251 (2021)

[21] Liu Y M, Wang K, Xu Q, Zhang J, Hu Y Z, Ma T B, Zheng Q S, Luo J B. Superlubricity between graphite layers in ultrahigh vacuum. *ACS Appl Mater Interfaces* **12**(38): 43167–43172 (2020)

[22] Sun J H, Zhang Y N, Lu Z B, Xue Q J, Wang L P. Attraction induced frictionless sliding of rare gas monolayer on metallic surfaces: An efficient strategy for superlubricity. *Phys Chem Chem Phys* **19**(18): 11026–11031 (2017)

[23] Ge X Y, Li J J, Luo J B. Macroscale superlubricity achieved with various liquid molecules: A review. *Front Mech Eng* **5**: 2 (2019)

[24] Cui Y X, Ding M, Sui T Y, Zheng W, Qiao G C, Yan S, Liu X B. Role of nanoparticle materials as water-based lubricant additives for ceramics. *Tribol Int* **142**: 105978 (2020)

[25] Li J J, Zhang C H, Deng M M, Luo J B. Reduction of friction stress of ethylene glycol by attached hydrogen ions. *Sci Rep* **4**: 7226 (2014)

[26] Han T Y, Yi S, Zhang C H, Li J J, Chen X C, Luo J B, Banquy X. Superlubrication obtained with mixtures of hydrated ions and polyethylene glycol solutions in the mixed and hydrodynamic lubrication regimes. *J Colloid Interface Sci* **579**: 479–488 (2020)

[27] Han T Y, Zhang C H, Luo J B. Macroscale superlubricity enabled by hydrated alkali metal ions. *Langmuir* **34**(38): 11281–11291 (2018)

[28] Li J J, Cao W, Wang Z N, Ma M, Luo J B. Origin of hydration lubrication of zwitterions on graphene. *Nanoscale* **10**(35): 16887–16894 (2018)

[29] Han T Y, Zhang C H, Li J J, Yuan S H, Chen X C, Zhang J Y, Luo J B. Origins of superlubricity promoted by hydrated multivalent ions. *J Phys Chem Lett* **11**(1): 184–190 (2019)

[30] Jia W P, Bai P P, Zhang W L, Ma L R, Meng Y G, Tian Y. On lubrication states after a running-in process in aqueous lubrication. *Langmuir* **35**(48): 15435–15443 (2019)

[31] Briscoe W H, Titmuss S, Tiberg F, Thomas R K, McGillivray D J, Klein J. Boundary lubrication under water. *Nature* **444**(7116): 191–194 (2006)

[32] Mutyala K C, Doll G L, Wen J G, Sumant A V. Superlubricity in rolling/sliding contacts. *Appl Phys Lett* **115**(10): 103103 (2019)

[33] Tortora A M, Halenahally Veeregowda D. Effects of two sliding motions on the superlubricity and wear of self-mated bearing steel lubricated by aqueous glycerol with and without nanodiamonds. *Wear* **386–387**: 173–178 (2017)

[34] Han T Y, Zhang C H, Chen X C, Li J J, Wang W Q, Luo J B. Contribution of a tribo-induced silica layer to macroscale superlubricity of hydrated ions. *J Phys Chem C* **123**(33): 20270–20277 (2019)

[35] Fang Y, Ma L R, Luo J B. Modelling for water-based liquid lubrication with ultra-low friction coefficient in rough surface point contact. *Tribol Int* **141**: 105901 (2020)

[36] Zhou Y, Qu J. Ionic liquids as lubricant additives: A review. *ACS Appl Mater Interfaces* **9**(4): 3209–3222 (2017)

[37] Amann T, Gatti F, Oberle N, Kailer A, Rühe J. Galvanically induced potentials to enable minimal tribochemical wear of stainless steel lubricated with sodium chloride and ionic liquid aqueous solution. *Friction* **6**(2): 230–242 (2018)

[38] Ge X Y, Li J J, Zhang C H, Wang Z N, Luo J B. Superlubricity of 1-ethyl-3-methylimidazolium trifluoromethanesulfonate ionic liquid induced by tribochemical reactions. *Langmuir* **34**(18): 5245–5252 (2018)

[39] Jiang C, Wang Y N, Su H G, Li W M, Lou W J, Wang X B. Synthesis and evaluation of a protic ionic liquid as a multifunctional lubricant additive. *Friction* **8**(3): 568–576 (2020)

[40] Su T, Song G J, Zheng D D, Ju C, Zhao Q. Facile synthesis of protic ionic liquids hybrid for improving antiwear and anticorrosion properties of water–glycol. *Tribol Int* **153**: 106660 (2021)

[41] Li W, Kumara C, Luo H, Meyer H M, He X, Ngo D, Kim S H, Qu J. Ultralow boundary lubrication friction by three-way synergistic interactions among ionic liquid, friction modifier, and dispersant. *ACS Appl Mater Interfaces* **12**(14): 17077–17090 (2020)

[42] Dong R, Bao L Y, Yu Q L, Wu Y, Ma Z F, Zhang J Y, Cai M r, Zhou F, Liu W M. Effect of electric potential and chain length on tribological performances of ionic liquids as additives for aqueous systems and molecular dynamics simulations. *ACS Appl Mater Interfaces* **12**(35): 39910–39919 (2020)

[43] Wang Y R, Yu Q L, Cai M R, Shi L, Zhou F, Liu W M. Ibuprofen-based ionic liquids as additives for enhancing the lubricity and antiwear of water-ethylene glycol liquid. *Tribol Lett* **65**: 55 (2017)

[44] Huang G W, Yu Q L, Ma Z F, Cai M R, Zhou F, Liu W M. Oil-soluble ionic liquids as antiwear and extreme pressure additives in poly-α-olefin for steel/steel contacts. *Friction* **7**(1): 18–31 (2019)

[45] Watanabe S, Pilkington G A, Oleshkevych A, Pedraz P, Radiom M, Welbourn R, Glavatskih S, Rutland M W. Interfacial structuring of non-halogenated imidazolium ionic liquids at charged surfaces: Effect of alkyl chain length. *Phys Chem Chem Phys* **22**(16): 8450–8460 (2020)

[46] Ito T, Aoki N, Tsuchiya A, Kaneko S, Akiyama K, Uetake K, Suzuki K. Detection of stress hormone in the milk for animal welfare using QCM method. *J Sens* **2017**: 6486891 (2017)

[47] Li J J, Zhang C H, Luo J B. Superlubricity achieved with mixtures of polyhydroxy alcohols and acids. *Langmuir* **29**(17): 5239–5245 (2013)

[48] Li J J, Zhang C H, Ma L R, Liu Y H, Luo J B. Superlubricity achieved with mixtures of acids and glycerol. *Langmuir* **29**(1): 271–275 (2013)

[49] Li J J, Zhang C H, Luo J B. Superlubricity behavior with phosphoric acid-water network induced by rubbing. *Langmuir* **27**(15): 9413–9417 (2011)

[50] Li J J, Zhang C H, Sun L, Lu X C, Luo J B. Tribochemistry and superlubricity induced by hydrogen ions. *Langmuir* **28**(45): 15816–15823 (2012)

[51] Czechowski G, Rabiega A, Jadzyn J. The viscous properties of diols. III. 1,2- and 1,4-butanediol in water and 1-pentanol. *Z Naturforsch A* **58**(9–10): 569–572 (2003)

[52] Hooke C J. The elastohydrodynamic lubrication of heavily loaded point contacts. *J Mech Eng Sci* **22**(4): 183–187 (1980)

[53] Ren X Y, Yang X, Xie G X, Luo J B. Black phosphorus quantum dots in aqueous ethylene glycol for macroscale superlubricity. *ACS Appl Nano Mater* **3**(5): 4799–4809 (2020)

Dapeng FENG. He received his Ph.D. degree in physical chemistry in 2001 from the Lanzhou Institute of Chemical Physics, Chinese Academy of Sciences (CAS), China. He is a professor at the State Key Lab of Solid Lubrication in the Lanzhou Institute of Chemical Physics, CAS. He has authored or co-authored more than 80 journal papers. His research interests are high performance lubricating oil, grease, and additives. He has gained a number of awards including "Second prize of National Technical Invention" and "Technology Invention Award of Gansu Province".

Dan QIAO. She received her Ph.D. degree in material science in 2014 from the Lanzhou Institute of Chemical Physics, CAS, China. She is an associate professor at the State Key Laboratory of Solid Lubrication in the Lanzhou Institute of Chemical Physics, CAS, China. She has authored or co-authored more than 30 journal papers. Her research interests are ionic liquids lubricants and tribology chemistry.

Zhiwen ZHENG. He received his B.S. degree in 2016 from the China University of Mining and Technology (in Xuzhou, China). He got his M.S. degree in 2019 from the Lanzhou Institute of Chemical Physics, CAS, China. Now, he is a Ph.D. candidate in the Lanzhou Institute of Chemical Physics, CAS, China. His current scientific interests are devoted to macroscale liquid superlubricity and novel lubricating additives.

Xiaolong LIU. He received his M.S. degree in 2019 from the Shandong Normal University, China. Now, he is an intermediate engineer in the Lanzhou Institute of Chemical Physics, CAS, China. His scientific interests mainly focus on the design, preparation, and tribo-chemistry of high-performance lubricant.

Hongxiang YU. He received his B.S. degree in 2018 from the Shandong Normal University, China. Now, he is a Ph.D. candidate at the Lanzhou Institute of Chemical Physics, CAS, China. His current scientific interests are devoted to mechanism and kinetic analysis of tribochemical reaction of lubricants, as well as novel lubricant additives.

Haijie CHEN. She received her B.S. degree in 2017 from the Shandong Normal University, China. Then, she entered the Lanzhou Institute of Chemical Physics, CAS, China, for a postgraduate and doctoral program. Now, she is a Ph.D candidate. Her ongoing research focuses on assembly lubrication film of 2D materials.